O T E C
Vol.25 (2020), 33 ~ 45

Numerical simulation of pressure pulsation in vane area of a pump-turbine at pump mode

Yao GUO[*1], Pengcheng GUO[*1], Yoichi KINOUE[*2], Longgang SUN[*1]

*1 State Key Laboratory of Eco-hydraulics in Northwest Arid Region of China,
Xi'an University of Technology, Xi'an 7, 10048, China
*2 Institute of Ocean Energy, Saga University, 840-8502, Japan

Abstract

When a reversible pump-turbine is running under the low-flow conditions in pump mode, it is easy to produce low-frequency and high-amplitude pressure pulsation, which affects the stability of the unit. In order to study the pressure pulsation characteristics of guide vane and stay vane passage during pump operation, this paper takes a power station pump-turbine model as research object, based on the SST k-ω turbulence model for its internal transient flow, a three-dimensional unsteay simulation of the whole flow channel is carried out. The results show that in hump zone, the first main frequency of the pressure pulsation in guide vane and bladeless zone is 0.2 times the rotation frequency, and the second main frequency is the blade passing frequency and its multiple. When flow rate is increased to the best efficiency conditions, the 0.2 times rotation frequency pulsation amplitude is disappeared. The main frequency of the pressure pulsation in vane channel and the vaneless zone is the blade passing frequency and its multiples. In order to clarify the reason for the high-amplitude pressure pulsation at the 0.2 times rotation frequency, the internal flow field of the hump zone was further analyzed based on the velocity coefficient. It was found that there are almost evenly distributed three stall groups in guide vane and stay vane. The change rotates at a low speed in a counterclockwise circumferential direction. Finally, the Q criterion is used to identify the vortex structure of the cascade channel. There are flow vortices and spanwise vortices of different strengths in the cascade channels. These vortex structures continuously rotate counterclockwise at low speed over time and block the flow channel. This leads to the appearance of low frequency and high amplitude pressure pulsation of 0.2 times the rotation frequency.

Key words : pump – turbine, pump working condition, vane area, pressure pulsation, rotating stall

1. Introduction

In order to meet the needs of power system load regulation, pump-turbine often needs to change operating conditions and deviate from the design operating conditions (Nan W., 2008). When the unit is operating under non-design conditions, pressure pulsation is likely to occur, which will cause unit vibration and even damage the its flow-through components, which will seriously affect unit stability (Dongming G et al., 2018). When the unit is operating under turbine conditions, an "S" characteristic area appears on the characteristic curve (Zeng W et al., 2016). This area will make it difficult for the unit to connect to the power grid. Unlike operated under turbine conditions, when the unit is operated under pump conditions, the hump phenomenon may occur on flow-head curve, which seriously affects its stability. In addition, there are unstable flow phenomena such as rotating stall (Chunze Z., 2017) and flow separation (Li Z J., 2016) in pump mode. In summary, the stability requirements of pump operating conditions are more stringent, and the pressure pulsation problem needs to be analyzed in depth. Analyzing the pressure pulsation produced by the flow-through components of a pump-turbine operated under non-design conditions, and exploring the causes and characteristics of the pressure pulsation are of great significance to the stability of the unit.

In recent years, many experts and scholars have carried out relevant research work on the stability of a pump-turbine

Date of Manuscript Acceptance 2020.11.20
E-mail of corresponding author: guoyicheng@xaut.edu.cn

in pump operation condition. Guo L (2014), Deyou L (2018), Qifei L (2018), etc. carried out numerical simulations on a pump-turbine under non-design working conditions, and obtained the law of the propagation of pressure pulsation in the circumferential and flow directions. When studying the pump conditions, it was found that the amplitude of the pressure pulsation at guide vane, stay vane and the vaneless area is relatively high, which has a significant impact on the stability of the unit. When Yin J L et al. (2010) analyzed the velocity field of the cascade channel, they found that the hydraulic loss at guide vane and stay vane was relatively large, resulting in a positive slope area (ie, hump area) on the head-flow curve. Sun Y (2014), Ziwu G (2017), etc. studied the pressure pulsation of a pump-turbine when the guide vane opening is small and found that the pressure pulsation amplitude in the vaneless zone was much higher than that in other areas. R Hongjuan R et al. (2012) analyzed the pressure pulsation of the first hump zone condition of the near design condition, obtaining that the dominant frequency of the pressure pulsation in guide vane was 0.2 times rotation frequency of the unit, and that the pressure pulsation was caused by the bad flow of slab in guide vane channel, which is consistent with the results obtained by Giovanna Cavazzini (2018). YANG J et al. (2015) analyzed a pump-turbine under pump design conditions and small flow conditions and showed that there is 0.6625 times passing frequency of guide vane under these two conditions, and pointed out that the bad flow occurred in the U-shaped stay vane suction surface is the internal cause of the pressure pulsation. Under small flow conditions, there is a pressure pulsation of 0.335 times pass frequency of guide vane. This pressure pulsation is caused by the unstable flow at guide vane, but it does not conduct a more in-depth analysis of the bad flow under these two working conditions. In summary, the current research work on the pressure pulsation in vane area of the unit under the non-design working conditions of a pump-turbine pump is not yet complete, and the cause, characteristics and propagation law of pressure pulsation have not yet reached a unified understanding.

Based on the SST k-ω turbulence model, this paper firstly develops a full-flow three-dimensional unsteady simlution of a pump-turbine with different flow under pump conditions to discuss the frequency components and the internal causes of the pressure pulsation in the vane area.

2. Calculation model and numerical method

2.1 Physical model

The calculation takes a model pump-turbine of a pumped storage power station as the object. The three-dimensional full flow channel geometric model is shown in Figure 1. The model has five flow parts, the runner, draft tube, spiral case, guide vane and stay vanes. The solid model of the pump-turbine is established by the three-dimensional modeling software UG. When it is operated under pump conditions, the fluid flows in through draft tube and flows out through spiral case. The geometric parameters of the model are: runner inlet diameter D_1=553mm, outlet diameter D_2=251.98mm, runner blade number Z_b=9, guide vane height b_0=37.76mm, stay vane number Z_c=20, and the number of guide vane Z_0=20. In addition, the rated speed of the pump - turbine is 1150r/min, and guide vane opening used in the calculation is α=14°.

2.2 Computational domain meshing

The professional grid generation software ICEM is used to divide computational fluid domain grid of the model, and each flow component uses a hexahedral structured grid, as shown in Figure 2. When dividing the grid, the boundary layer grid near the wall of each flow component is locally encrypted, so that it can more effectively capture the flow state of boundary layer near the wall. At the same time, the quality of the grid is controlled not less than 0.3 and its angle is not less than 18° to ensure a high grid quality standard.

When the opening of guide vane is 14°, select the highest efficiency operating point in pump mode to perform steady simulation, gradually increase the number of grids, and select head and torque as the evaluation criteria, so as to verify grid independence. The numerical calculation results are shown in Figure 3. It can be seen that when the number of grid nodes is greater than 3.99 million, the change of calculated values of head and torque do not exceed 1% due to the increasing grid nodes. A precision grid can simulate actual flow more effectively and accurately, but the more grid nodes, the higher the computer resources and calculation cycle requirements for calculations. Therefore, 5.56 million grid nodes is selected in this paper. Among them, the grid nodes number of draft tube, runner, guide vane, stay vane and spiral case are 0.71 million, 2.07 million, 1 million, 1.06 million and 0.708 million respectively. The details of the grid quality are shown in Table 1.

The commercial software ANSYS CFX was used to perform a three-dimensional unsteady simulation of the full flow channel of the model pump - turbine. The turbulence model adopts the SST k-ω model, and dynamic and static interface of the unsteady calculation is set to the Transient Rotor Stator type. Draft tube is used as inlet, and the boundary condition is set as pressure; the spiral case is used as outlet, and the boundary condition is set as mass flow. The wall condition is set as no slip and no friction, and both the convection term and the turbulence term adopt the high-order solution format; the transient term adopts the second-order backward Euler format. In unsteady calculations, the size of time step setting is related to the convergence speed and the accuracy of the calculation results. In this paper, the impeller is set to rotate 1° at each time step, and corresponding time step is 4.4348×10^{-4} s. The maximum iteration of each time step is 10 steps, and the maximum value of the convergence residual is not more than 1.0×10^{-3}. It takes 360 steps for runner to rotate one round, and the calculation processing should be no less than 20 rotation cycles, and take the results of the last 5 cycles for analysis.

Fig.1 Geometrical model of a pump - turbine

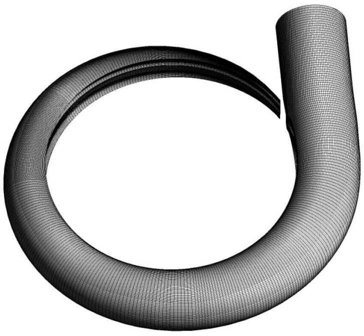

(a) Spiral case

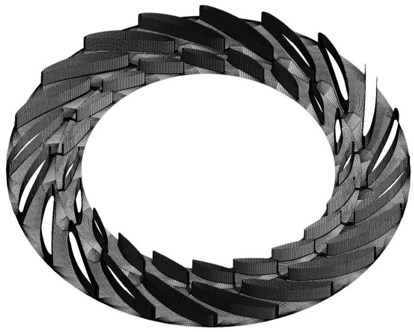

(b) Guide vane and stay vanes

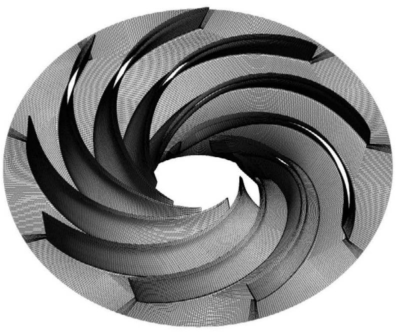

(c) Runner

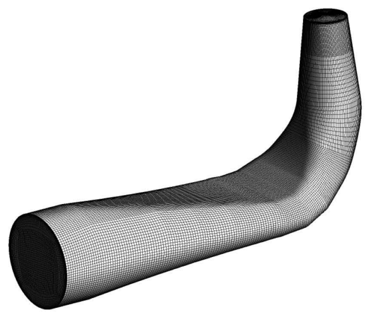

(d) Draft tube

Fig.2 The grids of each flow components

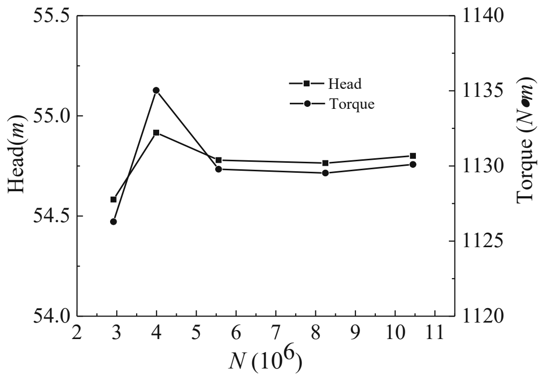

Fig.3 Grid independence analysis

Table 1 The number and quality of grid nodes of each flow component

	Guide Vane	Stay Vane	Runner	Draft Tube	Spairl Case	Total
Node Number	1063920	1001765	2075288	708920	710827	5560720
Grid Quality	0.5	0.46	0.5	0.3	0.35	

3. Analysis of calculation results

3.1 Experimental verification of numerical results

In order to verify the reliability of the numerical calculation, this paper carried out the model tests of the pump-turbine flow-efficiency and flow-head. In the tests, an electromagnetic flowmeter is used to record the flow, and a differential pressure sensor is used to measure the differential pressure between draft tube and spiral case and then to calculate the head. According to the IECS60193 Standard, the flowmeter, head differential pressure, main torque, friction torque and other sensors are calibrated within the test range using standard measuring instruments or instruments (1999). The random error and system error of the hydraulic efficiency of the model test bench are calculated according to Eq. (1) and Eq. (2),

$$E_{\eta_r} = \pm \frac{t_{0.95(N-1)} \times \sqrt{\sum (\eta_i - \overline{\eta})^2}}{\sqrt{N(N-1)} \times \overline{\eta}} \times 100\% \tag{1}$$

$$E_{\eta_s} = \pm \sqrt{E_Q^2 + E_H^2 + E_T^2 + E_n^2} \tag{2}$$

Where, N is the number of measurements, $t_{0.95}(N\text{-}1)$ is the t distribution value of (N-1) degrees of freedom corresponding to the 0.95 confidence probability, and η_i is the measured efficiency value of the i th of the experiment, $\overline{\eta}$ is the average efficiency. E_Q, E_H, E_T and E_n are the relative uncertainty of flow, head, torque and rotation speed, which are ±0.0853%, ±0.0759%, ±0.1416%, ±0.006% , respectively. After calculation, the random error and system error of hydraulic efficiency are ±0.0363% and ±0.182%, respectively, which meet the test requirements.

Figure 4 shows the comparison between the experimentally measured pressure coefficient as well as efficiency value and the numerical simulation. In the figure, the discharge coefficient φ and the head coefficient ψ are defined by Eqs.(3) and (4).

$$\varphi = \frac{Q}{\frac{\pi}{4} \times D^2 \times u} \tag{3}$$

$$\psi = \frac{2 \times g \times H}{u^2} \tag{4}$$

Where, D is the inlet diameter of a pump-turbine on pump mode whose unit is 'm'; n is the speed of a pump-turbine whose value is 1150 r/min; Q is the flow rate of a pump–turbine whose unit is 'm^3/s'; u is circumferential velocity at the inlet of runner under pump conditions whose unit is 'm/s'; H is the head of a pump – turbine whose unit is 'm'.

Figure 4 shows that numerical calculation results are in good agreement with the experimental results. Moreover, as the flow changes, numerical results of the pressure coefficient and efficiency are basically consistent with experimental values. However, the head result obtained by numerical calculation is higher than the test result as a whole, and as the flow rate increases, the difference gradually increases. The numerical calculation result of efficiency is also higher than the test result. The occurrence of these phenomena may due to factors such as mechanical loss caused by bearing friction which is not considered in the simulation, improper sealing and volume loss caused by blade tip clearance.

Table 2 reflects the pressure coefficient error and efficiency error at each operation condition point when compared with experimental results. At 14° guide vane opening, the best efficiency point in the numerical simulation results is named the optimal working condition point written as Q_b. It can be seen that the pressure coefficient error of numerical calculation does not exceed 3.15%, and the efficiency error value does not exceed 3.70%. Therefore, the numerical calculation method used in this paper has high reliability.

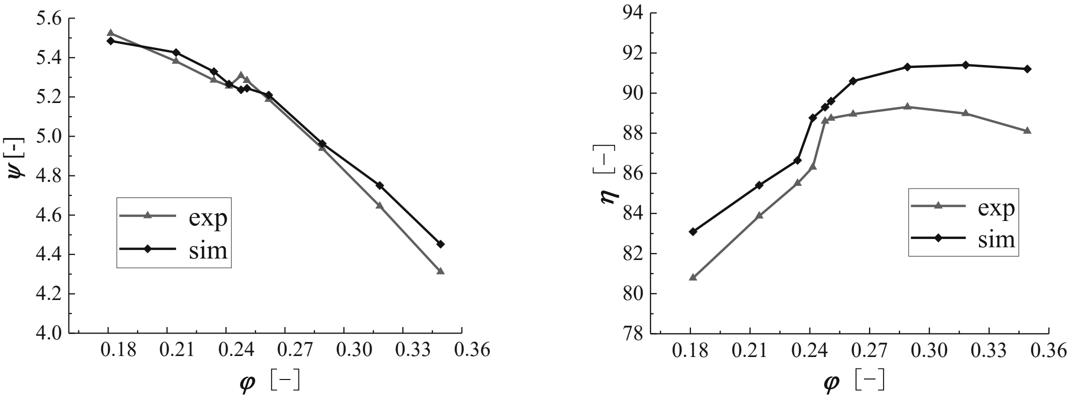

(a) Head-flow curve (b) Efficiency-flow curve

Fig.4 External characteristic curve of water pump turbine

This paper analyzes the small flow conditions at 14° guide vane opening, that is 0.76Q_b operating condition (Op1), hump zone operating condition 0.78Q_b (Op2) and the best efficiency point Q_b (Op3), the details of operating point are shown in Table 2.

Table 2 Parameters of operating condition point of at 14° guide vane opening

Conditions	Flow Coefficient φ	Flow	pressure coefficient error (%)	efficiency error (%)	description
Op1	0.24147	0.76Q_b	0.21	2.76	small flow operating condition
Op2	0.24763	0.78Q_b	-1.40	0.78	hump zone operating condition （CFD）
Op3	0.31822	Q_b	2.20	3.70	best efficiency point（CFD）

3.2 Settings of monitoring points

When a pump-turbine is operating under pump conditions, the hydraulic loss of vane channel and vaneless zone accounts for a large proportion, and the pressure pulsation is more obvious (Leqin W et al., 2013, Chunze Z et al., 2017).

In order to analyze the pressure pulsation of guide vane, stay vane, and vaneless area between runner and guide vane, 27 pressure monitoring points are set along the flow direction. The monitoring points distributes in the vaneless area between runner and guide vane, guide vane and stay vane. The first number after the monitoring point name represents the position on the spanwise surface. The surface close to Span 0.02 is 0, the surface Span0.5 is 1, and the surface Span0.98 is 2. The second number represents the position of the monitoring point in the flow direction, as shown in Figure 5.

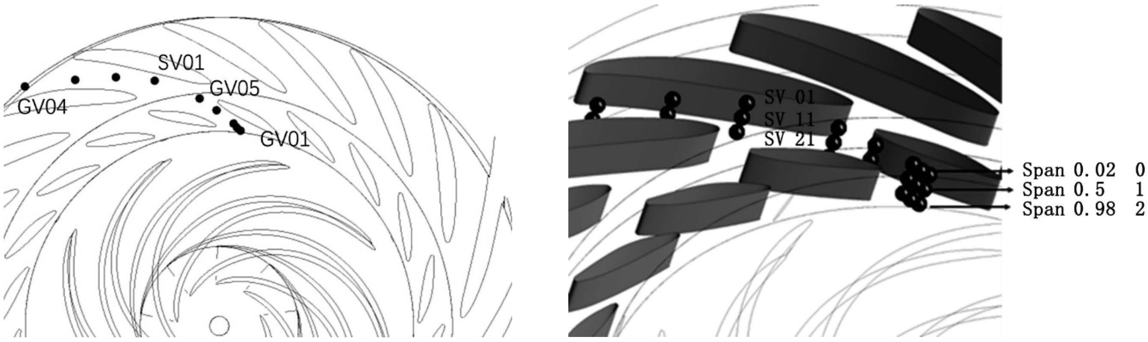

Fig.5 The distribution of monitoring point

3.3 Distribution of average pressure and standard deviation of pressure in guide vane and stay vane

The average pressure and pressure standard deviation of each monitoring point are shown in Figure 6. The abscissa of Figure 6 represents the serial number of the monitoring points (i. e., GV01-GV25 in guide vane or SV01-SV25 in stay vane). The pressure standard deviation can reflect the magnitude of pressure pulsation at each monitoring point. In the Op1 working condition, the average pressure and standard deviation of pressure at the monitoring points GV01-GV25 are shown in Figure 6(a). On the hub side, the middle spanwise surface and the shroud side, the average pressure of the monitoring points is almost equal. As the distance between the monitoring points and the runner increases, the average pressure first increases and then decreases. The average values of pressure at the tail of guide vane (GV04, GV14, GV24) are the largest. The value of pressure standard deviation is the largest in the middle spanwise surface, and the pressure standard deviations at the hub side and the shroud side are almost the same. The value of the pressure standard deviation decreases as the distance between the monitoring points and the runner increases.

The average pressure and pressure standard deviation of stay vane channel monitoring points SV01-SV24 are shown in Figure 6(b). Along the flow direction, the average value of pressure is proportional to the distance between the monitoring points and the guide vane, that is, the farther the monitoring points are from the guide vane, the greater the average pressure value. However, the pressure standard deviation is the opposite. The closer to the vaneless area, the greater the pressure standard deviation of the monitoring point, that is, the greater the pressure pulsation amplitude. In the axial direction, the average pressure and standard deviation of the pressure at the monitoring points at the shroud side, the middle spanwise surface and the hub side are almost equal.

The average pressure and standard deviation of pressure at the monitoring points of the guide vane under the Op2 condition are shown in Figure 6(c). Compared with the Op1 condition, the average value of pressure of the guide vane monitoring points increases, while the pressure standard deviation amplitude increases sharply. Under this condition, the farther the monitoring point is from the runner, the larger the average pressure value and the smaller the pressure standard deviation. Among the three planes, the average pressure and the pressure standard of the middle spanwise surface are the largest.

The average pressure and pressure standard deviation of the stay guide vane channel monitoring points SV01-SV24 are shown in Figure 6(d). Compared with Op1 condition, the pressure standard deviation of each monitoring point increases significantly. Along the flow direction, as the distance between the monitoring point and the guide vane increases, the average pressure gradually increases, while the pressure standard deviation gradually decreases. Along the axial direction, except for the stay vane inlet monitoring point on the shroud side (GV21), the pressure standard deviation is the largest. On the middle span, the pressure standard deviation of the other monitoring points is the largest.

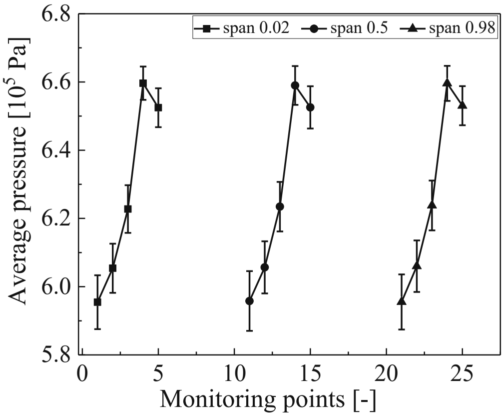

(a) Monitoring points in guide vane under Op1 condition

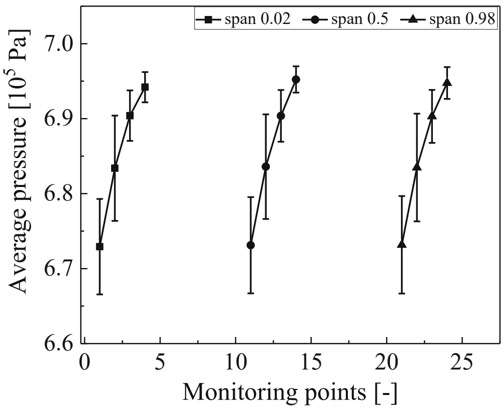

(b) Monitoring points in stay vane under Op1 condition

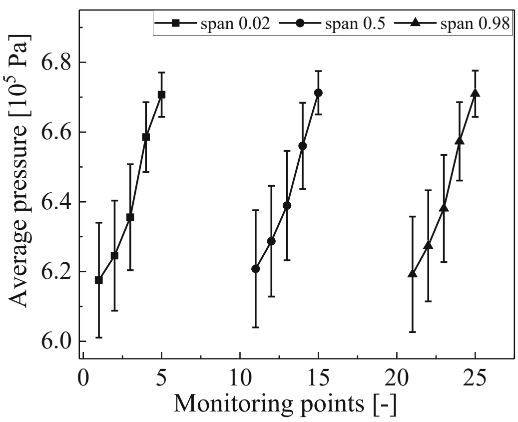

(c) Monitoring points in guide vane under Op2 condition

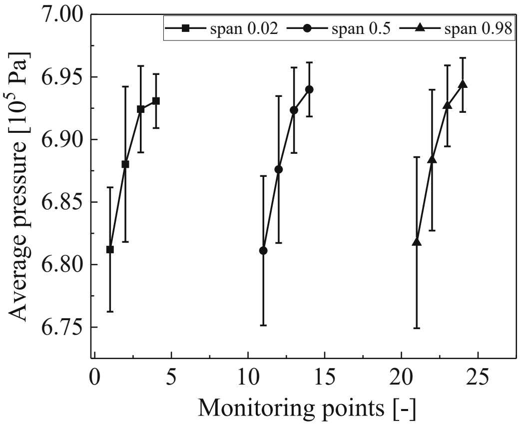

(d) Monitoring points in stay vane under Op2 condition

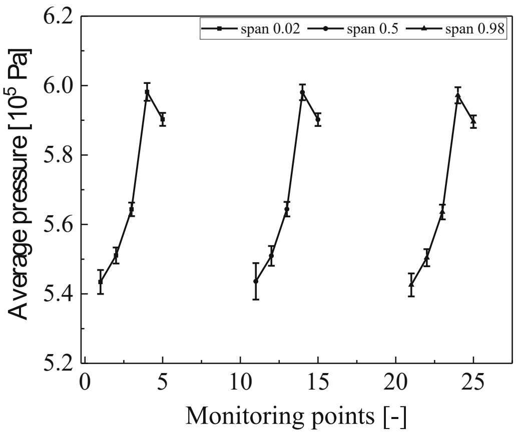

(e) Monitoring points in guide vane under Op3 condition

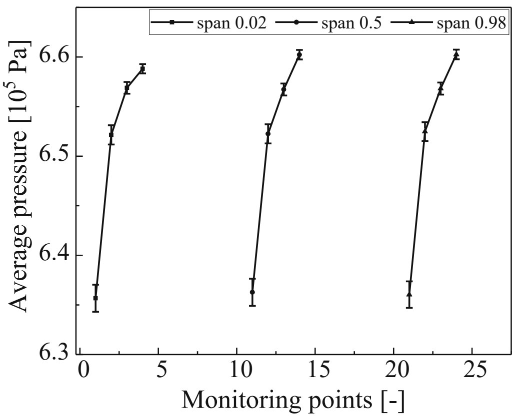

(f) Monitoring points in stay vane under Op3 condition

Fig. 6 The average pressure and the pressure deviation of monitoring points

When the flow increases to Q_b (i. e., under condition Op3), the average pressure and pressure standard deviation of each monitoring point of guide vane are shown in Figure 6(e). Compared with the previous operating condition, the average pressure and the pressure standard deviation of each monitoring point are further reduced. As the distance between the monitoring point and runner increases, the average pressure value first increases and then decreases, however, the pressure standard deviation first decreases and then increases. In the axial direction, the average pressure of the monitoring points on the three planes are nearly equal, but the difference in the pressure standard of the monitoring points in the middle spanwise plane is slightly larger than that of the other two planes. The average pressure and pressure standard deviation of the stay guide vane channel monitoring points are shown in Figure 6(f). As the flow increases, the average pressure and the pressure standard deviation of the monitoring points decrease. Along the flow direction, as the distance between the monitoring point and the guide vane increases, the average pressure increases, while the pressure standard deviation gradually decreases. In the axial direction, the average pressures and standard deviations of the three planes are not much different. The pressure standard deviations on the hub side are slightly larger than the other two planes.

To sum up, for the same operating point, the pressure pulsation amplitudes of the three plane monitoring points on the hub side, the shroud side and the middle spanwise surface are not much different, but the pressure pulsation amplitude on the middle spanwise surface is slightly larger than the pressure pulsation amplitude of the other two planes. For the monitoring points, the closer to the vaneless area between the runner and the guide vane, the smaller the average pressure, but the greater the pressure pulsation amplitude.

3.4 Analysis of pressure pulsation in guide vane and stay vane

Based on the analysis above, fast Fourier transform (FFT) is performed on the pressure data collected by the monitoring point on the middle spanwise surface to analyze its frequency domain characteristics. Figure 7 shows the frequency spectrum of the pressure pulsation at the monitoring point on the middle spanwise surface under 4 working conditions. In the Op1 condition, the pressure spectrogram of the guide vane monitoring points GV11-GV15 is shown in Figure 7(a). The first main frequency of each monitoring point is $0.2f_n$ (f_n is the rotation frequency), followed by $9f_n$ (the blade passing frequency). Among them, from the inlet to the outlet of guide vane, the amplitude of $0.2f_n$ first increases and then decreases, and the maximum value appears at GV13 (the middle of guide vane) while the minimum value appears at the GV15 (between guide vane and stay vane). The second main frequency $9f_n$ is caused by the rotor and stator interference(RSI) between runner and guide vane. The farther the monitoring point is from runner, the less it is affected by the RSI, and the smaller the pulsation amplitude. The pressure spectrogram of the stay vane channel monitoring points SV11-SV14 is shown in Figure 7(b), the main frequency is also $0.2f_n$, and the second main frequency is $18f_n$ (2 times of the blade passing frequency). The frequency $0.2f_n$ has the largest amplitude at the monitoring point SV12 (the middle of stay vane channel); from stay vane inlet to outlet, the amplitude of $18f_n$ gradually decreases. Comparing Figure 7 (a) with Figure 7 (b), the dominant frequency of this operating condition is $0.2f_n$, and the amplitude is the largest near the middle of guide vane.

When the flow increases to the Op2 working condition, the dominant frequency of each monitoring point is also $0.2f_n$. Compared with the Op1 working condition, the amplitude of guide vane monitoring point $0.2f_n$ increases significantly, as shown in Figure 7(c). The first dominant frequency of guide vane channel is $0.2f_n$, and the trend of its amplitude is consistent with that of the Op1 condition, and the amplitude at GV13 is the largest. The second main frequency is $9f_n$ (blade passing frequency), and its amplitude gradually decreases from inlet to outlet of the guide vane, and the amplitude is the largest at GV11. The pressure pulsation spectrum of stay vane monitoring point is shown in Figure 7(d). The first dominant frequency is $0.2f_n$, and its amplitude is much smaller than that of guide vane monitoring point. The second main frequency is $18f_n$, and SV11 has the largest amplitude. Compared with Fig. 7(c) and (d), the main frequency of this condition is still $0.2f_n$, and the amplitude is the largest at guide vane monitoring point GV13. In the Op3 working condition, the pressure pulsation amplitude of each monitoring point is significantly reduced. The first main frequency is changed from $0.2f_n$ to $18f_n$, which is caused by the rotor and stator interference of runner and guide vane. The second main frequency is $9f_n$, and the pulsation amplitude of the low-frequency component $0.2f_n$ at the monitoring point of the vane channel decreases sharply or even disappears.

To sum up, in Op3 (the highest efficiency condition), the dominant frequency at guide vane and stay vane is $18f_n$, which is twice the blade passing frequency; in Op1 (small flow condition) and Op2 (hump zone operating condition), the dominant frequency of the pressure pulsation at guide vane and stay guide vane is $0.2f_n$, which is consistent with the experimental results of Hongjuan R et al., (2012). In order to explore the reason for the $0.2f_n$ low-frequency pressure pulsation, the internal flow field at the Op2 (that is, $0.78Q_b$ condition) is further analyzed.

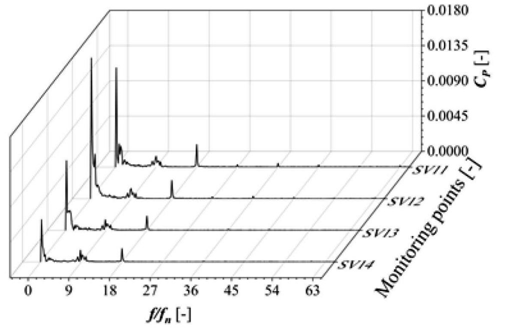

(a) Monitoring points in guide vane under Op1 condition

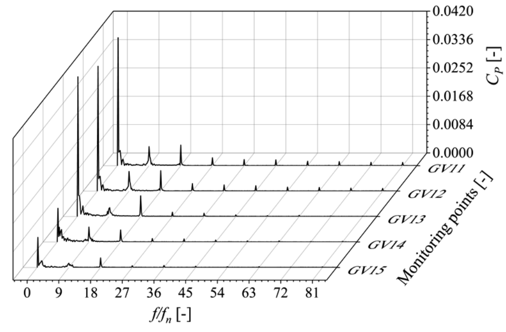

(b) Monitoring points in stay vane under Op1 condition

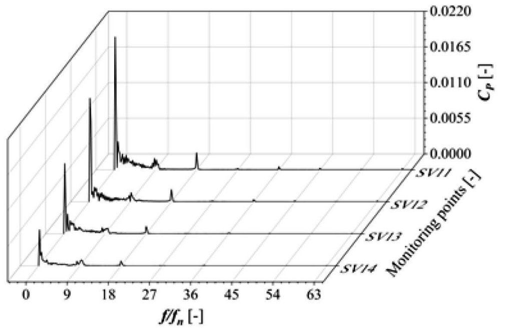

(c) Monitoring points in guide vane under Op2 condition

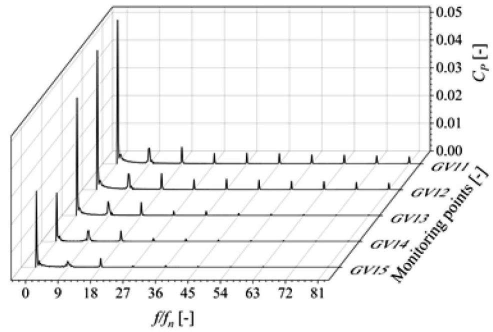

(d) Monitoring points in stay vane under Op2 condition

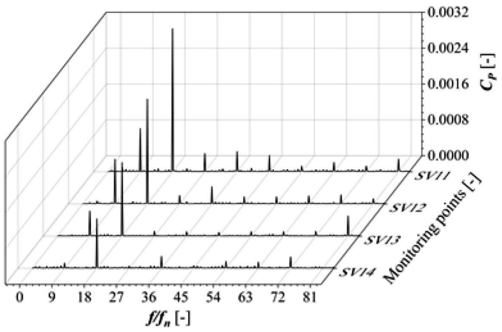

(e) Monitoring points in guide vane under Op3 condition

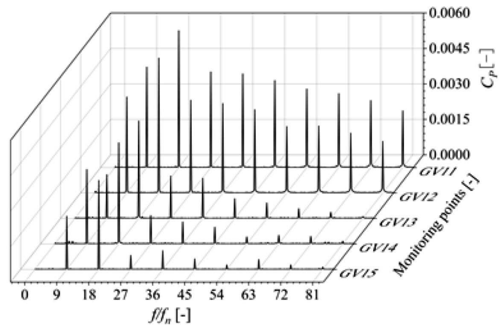

(f) Monitoring points in stay vane under Op3 condition

Fig. 7 Pressure spectrogram of monitoring point

3.5 Analysis of flow characteristics

Figure 8 shows the absolute velocity cloud diagrams of the runner and the guide vane channel and the evolution of the stall vortex at different times in the $0.78Q_b$ operating condition. In this figure, U_{st} is the velocity coefficient (Chunze Z et al., 2017), which is defined by Eq. (5).

$$U_{st} = \frac{V}{u} \tag{5}$$

Where, V is the instantaneous absolute velocity, and u is the circumferential velocity of runner outlet. It can be seen from the figure that three sets of stall clusters appeared in the circumferential direction of cascade channel composed of stay vanes and guide vanes, and these three sets of stall clusters are almost evenly distributed in the guide vanes and the stay vane channels. As time changes, the stall cluters rotates at low speed in the circumferential direction in a counterclockwise direction. Comparing Figure 8(a) and Figure 8(e), it can be seen that when the impeller rotates for five cycles (T_0+5T), the three sets of stall cluters all rotate 120° in the series cascade channel. The distribution is similar to that at $t=T_0$, so the low-speed rotating motion of these three set of rotating stall cluters is the internal cause of the $0.2f_n$ low-frequency and high-amplitude pressure pulsation in the series cascade channel.

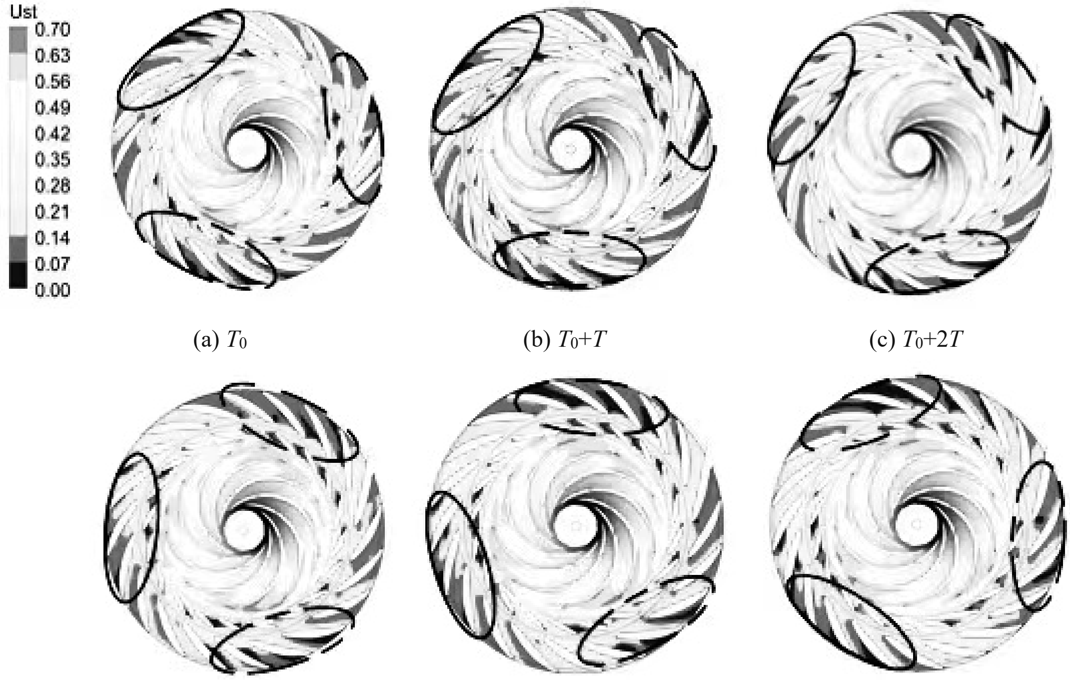

(a) T_0 (b) T_0+T (c) T_0+2T

(d) T_0+3T (e) T_0+4T (f) T_0+5T

Fig. 8 Absolute velocity pressure cloud diagrams in $0.78Q_b$ condition at different time

The vortex identification criterion can clearly and objectively reflect the vortex structure in complex flows (Yuning Z et al., 2018). In order to further clarify the characteristics of the internal rotating stall clusters of cascade channel, this paper adopts the Q criterion (ZHANG Y N et al., 2018) to identify the vortex structure appearing in the series cascade channel where the monitoring points are arranged. The Q criterion can simultaneously capture the strong and weak vortexes in the flow channel. According to the definition of Q criterion by Hunt et al.(1988), it is based on the decomposition of the local velocity tensor D_{ij}, which is defined by Eq. (6).

$$D_{ij}=S_{ij}+\omega_{ij} \tag{6}$$

Where, S_{ij} is the symmetric tensor, which represents the deformation part of the fluid; ω_{ij} is the antisymmetric tensor representing the rotating part of the fluid. The characteristic equation of D_{ij} is defined by Eq. (7).

$$\lambda^3 + P\lambda^2 + Q\lambda + R = 0 \tag{7}$$

Where, P, Q, R are three invariants related to the velocity tensor gradient. Q is defined by Eq. (8).

$$Q=\frac{1}{2}\left[tr\left(\overline{D}\right)^2 - tr\left(\overline{D}^2\right)\right]=\frac{1}{2}\left(\left\|\omega_{ij}\right\|^2 - \left\|S_{ij}\right\|^2\right) \tag{8}$$

When $Q>0$, the rotation of flow state in the flow channel is greater than the deformation of the flow state, that is, there is vortex motion.

The vorticity distribution on the middle spanwise surface of stay vane and guide vane in the $0.78Q_b$ condition is analyzed. Based on experience and combined with the actual flow characteristics in the flow channel, the Q value is selected as $15000\mathrm{S}^{-2}$ in this paper. Figure 9 shows the vortex structures of guide vane and stay vane channel at different times. Among them, the circle in the figure is the channel where the monitoring points are arranged. At time T_0, there are streamwise vortex and spanwise vortices at guide vane of channel A, and these vortex structures block the channel.

Streamwise vortex of different intensities appears in stay vane channel. At time T_0+T, the vortex flows counterclockwise to the next channel. There is still a vortex structure in channel A, but the streamlines at guide vane is smooth, and there is only a shedding vortex at the outlet. After two cycles (that is, t=T_0+2T), the streamlines at stay vanes and guide vanes of channel A are relatively smooth, and there is only a streamwise vortex at the inlet on suction surface of stay vane. At t=T_0+3T, the volume of the streamwise vortex at the inlet on suction surface of stay vane increases, and the spanwise vortex appears again at the outlet of the suction surface of guide vane. After four cycles, the volume of the spanwise vortex at guide vane of channel A increases, and the streamwise vortex also appears in the vaneless area between guide vane and stay vane. At T_0+5T, the vortex intensity of channel A is weakened, and the vortex structure is broadcast to the next channel. Comparing diagrams (a)-(f), it can be found that the vortex structures are circumferentially distributed in guide vane channel, blocking the flow channel, and rotating counterclockwise at low speed over time, resulting in the appearance of the 0.2f_n low frequency and high amplitude pressure pulsation.

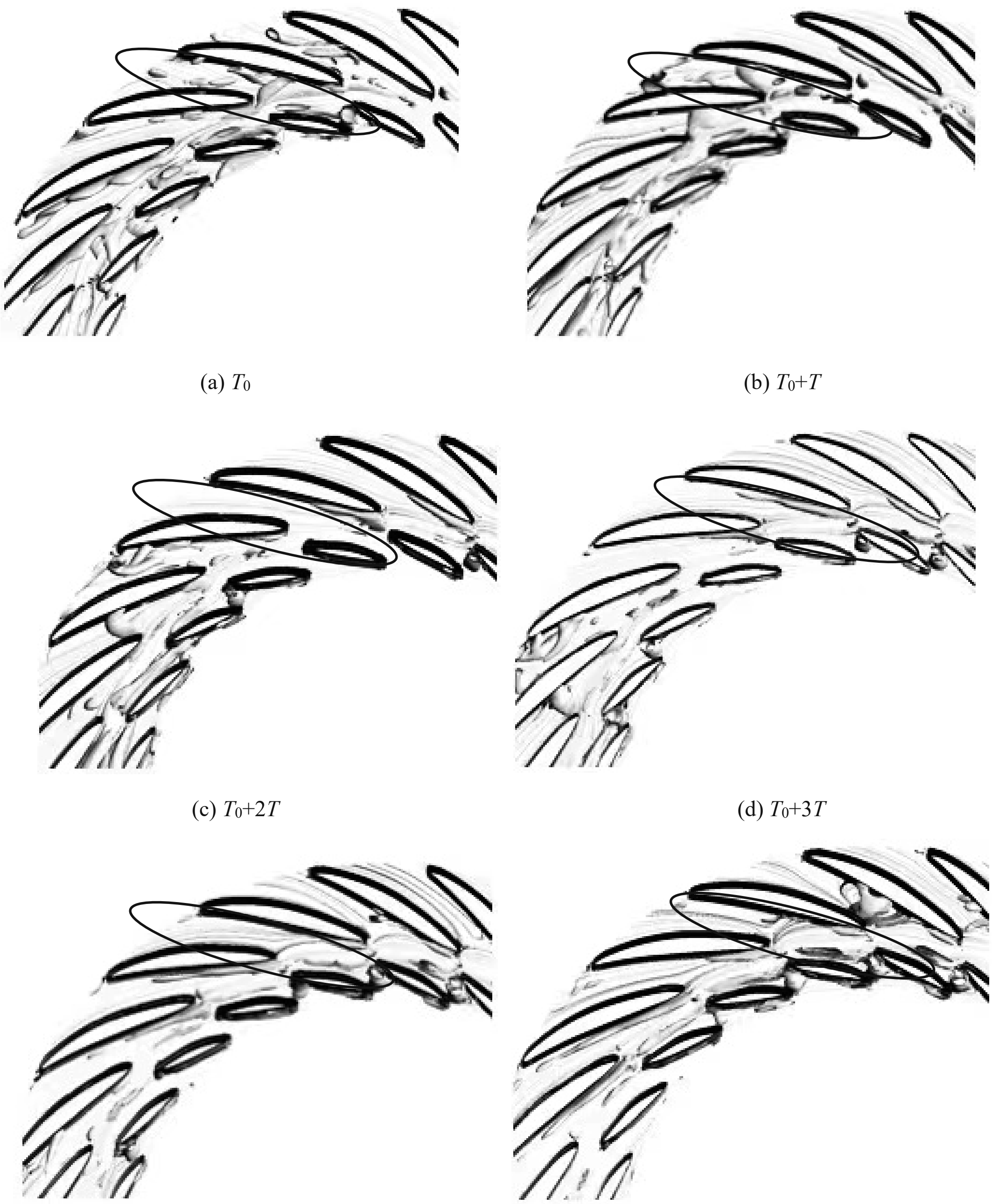

(a) T_0 (b) T_0+T

(c) T_0+2T (d) T_0+3T

(e) T_0+4T (f) T_0+5T

Fig. 9 Vortex structures in guide vane channel under 0.78Q_b condition at different time

4. Conclusion

In this paper, a model pump turbine of a pumped-storage power station is developed with unsteady simulation in the whole flow channel, and the guide vane channel is analyzed when the pump turbine is operated at the near hump area, hump area and the highest efficiency point. And the pressure pulsation at the vaneless zone, the conclusions are as follows: (1) The pressure pulsation amplitudes at the corresponding monitoring points on the three planes close to the hub side, the sproud side and the middle spanwise surface under the same working condition are nearly equal, and the pressure pulsation amplitude of the spanwise surface in the middle is slightly larger than the pressure pulsation amplitude of other two planes. (2) When the unit is operated at the highest efficiency point, the main frequency of the pressure pulsation at the monitoring point is $18f_n$, which is twice the blade passing frequency. The $18f_n$ frequency is caused by the static and dynamic interference between the runner and the guide vane. The second main frequency is $9f_n$; when in the near hump area and the hump area, the main frequency of the pressure pulsation at the monitoring point is $0.2f_n$, and the second main frequency is $9f_n$; (3) Analyzing the absolute velocity cloud diagrams of the runner and the guide vane channel at different times under $0.78Q_b$ conditions shows that the series cascade channel is almost evenly distributed with three rotating stall clusters. After the impeller rotates five cycles, the three stall clusters are all counterclockwise for 120°, at this time the absolute flow velocity cloud image is the same as when at the initial time. Finally, the Q criterion is used to identify the vortex structure of the rotating stall cluster in the series cascade channel, and it is found that there are vortexes of different shapes and different intensities in the series cascade channel. These vortex structures block the flow channel and continue to rotate counterclockwise at a low speed over time causeing the appearance of high amplitude and low frequency pressure pulsation at a frequency of $0.2f_n$.

Acknowledgement

This work was supported by the National Natural Science Foundation of China(Grant No. (51839010), the Key Research and Development Program of Shaanxi Province(Grant No. 2017ZDXM-GY-081) , The Youth Innovation Team of Shaanxi Universities(Grant No. 2020-29) and the cooperative Research Program of IOES(No.18A07).

References

Nan W., Current Situation and Prospects of the Pumped-Storage Power Plant in China, Vol. 20, No.2, (2008), pp. 18-20+70.

Chunze Z., Linsheng X., &Wei D., Influence of flow structures evolution on hump characteristics of a model pump-turbine in pump mode, Journal of Zhejiang University (Engineering Science), Vol. 51, No. 11, (2017), pp.162-171.

Li Z J., Wang Z W., &Wei X., Flow Similarity in the Rotor-Stator Interaction Affected Region in Prototype and Model Francis Pump-Turbines in Generating Mode, Journal of Fluids Engineering – Transactions of the ASME, Vol. 138, (2016), pp. 1-15.

Guo L., Liu J T., &Wang L Q., Pressure fluctuation propagation of a pump turbine at pump mode under low head condition, Science China Technological Sciences, 2014, 57(4):811-818.

Deyou L., Hongjie W., &Yonglin Q., Mechanism of high amplitude low frequency fluctuations in a pump-turbine in pump mode, Renewable Energy, Vol. 126, (2018), pp.668-680.

Qifei L., Yuankai W., &Chao L., Pressure fluctuation characteristics of Francis pump turbine in Hump zone, Journal of Drainage and Irrigation Machinery Engineering, Vol. 36, No.06, (2018), pp. 488-493.

Yin J L., Liu J T., &Wang L Q., Performance prediction and flow analysis in the vaned distributor of a pump turbine under low flow rate in pump mode, Sci China Tech Sci, Vol. 53, (2010), pp. 3302−3309.

Sun Y., Zuo Z., &Liu S., Distribution of Pressure Fluctuations in a Prototype Pump Turbine at Pump Mode, Advances in Mechanical Engineering, Vol.1, (2014), pp. 174-183.

Ziwu G., Demin L., &Yongzhi Z., CFD Research on Pressure Pulsation Characteristics of a Pump-turbine at Hump region in vaneless zone, Mechanical & Electrical Technique of Hydropower Station, Vol. 40, No.05, (2017), pp. 15-20+100.

Hongjuan R., Xianwu L., &Lei Z., Experimental study of the pressure fluctuations in a pump turbine at large partial flow conditions, Chinese Journal of Mechanical Engineering, Vol. 25, No. 6, (2012), pp. 1205–1209.

Giovanna Cavazzini., Jean-Bernard Houdeline., &Giorgio Pavesi., Unstable behaviour of pump-turbines and its effects on power regulation capacity of pumped-hydro energy Storage plants, Renewable and sustainable Energy Reviews, Vol.94 , (2018), pp. 399–409.

YANG J., PRAVESI G., &YUAN S., Experimental characterization of a pump-turbine in pump mode at hump instability region, Journal of Fluids Engineering, Vol.137, (2015), pp. 1–11.

Hydraulic Turbines, Storage Pumps and Pump Turbines-Model Acceptance Tests: IEC60193-1999[S]. International Electrotechnical Commission: Geneva, Switzerland, (1999).

Leqin W., Yingyuan L., &Liu Wanjiang., Pressure fluctuation characteristics of pump – turbine at pump mode, Journal of Drainage and Irrigation Machinery Engineering, Vol. 31, No.1, (2013), pp.7-10.

Chunze Z., Linsheng X., &Wei D., Pressure fluctuations characteristics and rotating stall propagation mechanism of a pump-turbine in pump mode, Journal of Hydraulic Engineering, Vol.48, No.7, (2017), pp. 837-845.

Yuning Z., Kaihua L., &Haizhen X., A review of methods for vortex identification in hydroturbines, Renewable and Sustainable Energy Reviews, Vol. 81, (2018), pp. 1269-1285.

ZHANG Y N., LIU K H., &LI J W., Analysis of the vortices in the inner flow of reversible pump turbine with the new omega vortex identification method, Journal of Hydrodynamics, VOL.30, No. 3, (2018), pp. 463-469.

HUNT J C R., WRAY A A., &MOIN P., Eddies, streams, and convergence zones in turbulent flows, Studying Turbulence Using Numerical Simulation Databases,Proceeding of the 1988 Summer Program, San Francisco, USA, (1988).